# Surface-plasmon-resonance-like fiber-based sensor at terahertz frequencies

**Alireza Hassani, Alexandre Dupuis, and Maksim Skorobogatiy***

*Génie physique, École Polytechnique de Montréal, C.P. 6079, succ. Centre-Ville, Montreal, Québec H3C3A7, Canada*
**Corresponding author: maksim.skorobogatiy@polymtl.ca*

Received May 14, 2008; revised July 28, 2008; accepted August 1, 2008;
posted August 7, 2008 (Doc. ID 96175); published September 30, 2008

Terahertz (THz) plasmonlike excitation on top of a thin ferroelectric polyvinylidene fluoride layer covering a solid-core polymeric Bragg fiber and facing liquid analyte is demonstrated theoretically. In a view of designing a fiber-based sensor of the analyte refractive index, phase matching of a THz plasmonlike mode with the fundamental core guided mode of a fiber is then demonstrated for the most challenging case of low refractive index analytes. A novel sensing methodology based on the core mode anomalous dispersion is proposed. Similarly to the surface plasmon resonance sensors in the visible, we show the possibility of designing high-sensitivity sensors in the THz regime with a resolution of $2\times10^{-4}$ in refractive index change. © 2008 Optical Society of America

*OCIS codes:* 130.6010, 240.6680, 060.2370, 040.2235, 060.5295.

## 1. INTRODUCTION

In the visible and ultraviolet range the collective oscillation of free charge carriers at a metal–dielectric interface yields a surface plasmon wave propagating along the surface of the metal [1–5]. The sensitivity of plasmon excitation to changes in the refractive index of the dielectric medium has been widely exploited for sensing applications. The plasma frequency, which imposes a lower frequency limit for the existence of these plasmons, is defined by $\omega_p^2=ne^2\varepsilon_0 m_e$, where $n$, $e$, $\varepsilon_0$, and $m_e$ are the electron density, electric charge, vacuum permittivity, and electron mass. Since the free electron density in metals is typically in the range of $10^{22}$ cm$^{-3}$, the plasma frequency is frequently limited to the visible and ultraviolet regions. At frequencies significantly below the plasma frequency [such as the terahertz (THz) range], large negative permittivity strongly prohibits electromagnetic fields from penetrating inside a metal, and plasmon excitation on the metal–dielectric interface becomes challenging. Therefore, efficient plasmonic excitation at lower frequencies requires materials with lower plasma frequencies [6–16]. Recently, Pendry *et al.* have suggested an artificial material in the form of a 2D subwavelength metallic wire lattice for which the effective plasma frequency is designable and equals $\omega_p^2=2\pi c^2a^2\ln(a/r)$ [15,16]. Since this plasmon frequency relies on the wire radius, $r$, and the lattice constant, $a$, the geometrical parameters of the artificial structure can tune the electron plasma frequency of metal to the THz or sub-THz frequency range. Moreover, further studies have recently confirmed that artificial subwavelength-sized metal structures can tune the plasma frequency of metals to the gigahertz or THz frequency range and allow metals to support plasmonlike surface waves at frequencies much lower than the visible range [6,7,10,13].

Alternatively, some materials can naturally support plasmonlike excitations in the THz regime due to resonances in their dielectric constant. Particularly, polyvinylidene fluoride (PVDF) is a ferroelectric semicrystalline polymer with a small absolute value of permittivity in the visible and near-IR regions. However, in the THz region the dielectric function of ferroelectric PVDF exhibits a resonance:

$$\varepsilon_{\mathrm{PVDF}}(\omega)=\varepsilon_{\mathrm{opt}}+\frac{(\varepsilon_{dc}-\varepsilon_{\mathrm{opt}})\omega_{TO}^2}{\omega_{TO}^2-\omega^2+i\gamma\omega}, \tag{1}$$

where, according to [17] $\varepsilon_{\mathrm{opt}}=2.0$, $\varepsilon_{dc}=50.0$, $\omega_{TO}=0.3$ THz, and $\gamma=0.1$ THz. Figure 1 shows the real and imaginary parts of the refractive index of ferroelectric PVDF in the wavelength range between 100 $\mu$m (3 THz) and 700 $\mu$m (0.43 THz). The real part of the refractive index of PVDF in this region is less than one, while the imaginary part is positive and mostly larger than one. Therefore, the real part of the PVDF dielectric constant is negative and by analogy with the behavior of the metals in the visible range, the PVDF layer is expected to support a plasmonlike excitation. Furthermore, PVDF gives an opportunity to design a fully polymeric structure for THz plasmonic devices using such established mass production techniques as microembossing and fiber drawing, which potentially makes the fabrication process highly suitable for the industrial scale-up.

This paper pursues two goals. The first is to show that layers of ferroelectric PVDF can support THz plasmonlike excitations similar to the ones found in metals in the visible range. The second is to show that, similarly to the design of surface plasmon resonance (SPR) sensors in the visible, we can design integrated fiber-based sensors in the THz regime, which are highly sensitive to the changes in the refractive index of the analyte. Practical implementation of the THz SPR-like sensor discussed in this work is a solid-core Bragg fiber with a PVDF layer on a top facing low refractive index analyte.

 

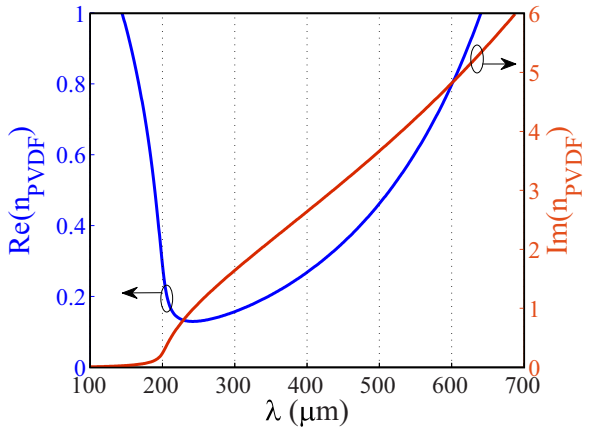


Fig. 1. (Color online) Real and imaginary part of the refractive index of ferroelectric PVDF.

## 2. TERAHERTZ PLASMONLIKE EXCITATIONS

We first would like to remind the reader of the general ideas behind the principles of operation of a fiber-based SPR sensor. A typical configuration of such a sensor is a fiber with a thin metal layer deposited on its surface in the near proximity of a fiber core. Another side of a metal layer is facing the analyte to be monitored. During operation of a sensor, one launches a broadband light into the fiber core. In the vicinity of a specific wavelength defined by the sensor design, one of the core modes is phase matched (avoiding crossing of the corresponding dispersion relations) with a plasmon excitation mode confined to the metal–analyte interface. In the vicinity of such a resonant wavelength one observes a dramatic decrease in the power transmitted through the fiber due to partial energy transfer from the core guided mode into a lossy plasmon. As the dispersion relation of a plasmon mode is very sensitive to the refractive index of an analyte, resonant wavelength, and, hence, spectral position of the absorption peak will shift when the analyte refractive index is changed. By detecting the spectral shift in the absorption peak of a core-guided mode, changes in the analyte refractive index of the order of $10^{-4}$–$10^{-5}$ refractive index units (RIU) can be detected.

Additionally, as detailed in [4,5], using photonic bandgap fibers considerably simplifies phase matching of the plasmon and core-guided fiber modes, especially in the case of low refractive index analytes. Particularly, the effective refractive index of a plasmon excitation is typically close to that of an analyte, while the effective refractive index of a core guided fiber mode is close to that of a core material. As there are few optical materials that have refractive indices smaller than 1.45, in practice it becomes challenging to achieve phase matching between the plasmon and core guided modes when the analyte refractive index is smaller than 1.4 (the case of gaseous and aqueous analytes). A key advantage of using the photonic bandgap fibers is that the fundamental core-guided mode in such fibers can be designed to have an arbitrarily small effective refractive index. Particularly, by placing the reflector bandgap at the desired wavelength of operation, and by adjusting the fiber core size, one can design a fundamental core mode to have arbitrarily small effective refractive index, and to achieve phase matching with a plasmon mode at any desired operational wavelength and for any analyte.

In this paper, we demonstrate the possibility of THz plasmoniclike excitation on top of a PVDF layer facing a low refractive index liquid analyte with $n=1.33$. A plasmonlike mode is excited by the fundamental mode of a solid-core Bragg fiber at the frequency of phase matching between the two modes. The Bragg fiber detailed here is assumed to have a solid core made of polymethyl methacrylate (PMMA) (refractive index $n_{\mathrm{PMMA}}=1.59$ at 1 THz), and surrounded with three bilayers of polycarbonate (PC) (refractive index $n_{\mathrm{PC}}=1.65$ at 1 THz) and PMMA, thus forming a Bragg reflector [18]. The core radius is $R_c=300$ $\mu$m; the thicknesses of the PC and PMMA layers are 130 and 205 $\mu$m, respectively. A 10 $\mu$m thick ferroelectric PVDF layer is placed on top of the Bragg reflector. Figure 2(a) presents a schematic of the proposed solid-core THz Bragg fiber. The PMMA–PC thicknesses were chosen so that the center wavelength of the Bragg reflector bandgap is near 280 $\mu$m (~1 THz).

When operating within the bandgap of a Bragg fiber reflector, the fields of a fundamental Gaussian-like $HE_{11}$ leaky core mode decay exponentially fast into the periodic reflector. Therefore, modal field intensity in the PVDF layer also decreases exponentially fast with the number of layers in the reflector. Therefore, the total number of bilayers must remain small in order for the light to be able to couple to a plasmon. It is important to note that in this first study the material absorption was considered only in the PVDF layer. As we will see further, this choice is justified as loss incurred due to coupling to a plasmon excitation, generally, is much higher than the loss due to absorption of the fiber materials. Therefore, to simplify interpretation of the results we set fiber material losses to zero.

We used a finite-element method with perfectly matched layer boundaries and a fourfold symmetry [19] in order to find the complex propagation constants of the core-guided and plasmonic modes by solving the vectorial Maxwell equations. In a particular case of fibers exhibiting circular symmetry, the results produced by the finite

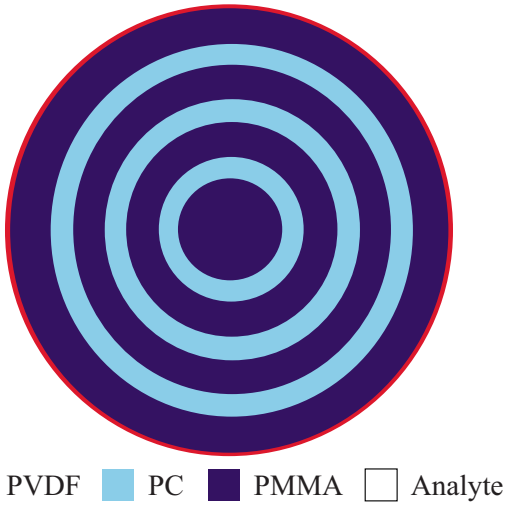


Fig. 2. (Color online) Schematic of a solid-core THz Bragg fiber with PVDF layer facing analyte.

element method can be also confirmed by a transfer matrix method. Since we have neglected material absorption, the imaginary part of the core mode propagation constant defines modal propagation loss resulting from coupling to a lossy plasmon. For a given analyte, we design a Bragg fiber reflector in such a manner as to ensure that the effective refractive index of a plasmonic excitation (which is close to that of the analyte) falls within the fiber bandgap. We then vary the fiber core size to position the core-guided mode dispersion curve in such a way as to phase match it with a plasmon mode. Sensing in analytes of significantly different refractive indices requires distinct fiber designs. In all the simulations that follow we arbitrarily assume a low refractive index analyte with refractive index of $n=1.33$. Nevertheless, design considerations presented in this paper are general and can be adapted to any analyte refractive index.

Figure 3 shows the dispersion relation of the fundamental core mode, and the plasmonic mode. The solid and dashed black curves (blue online) present the dispersion relations of the fundamental core mode for the two values of the analyte refractive index of 1.33 and 1.335, respectively. Furthermore, Fig. 4 shows the field distributions in various fiber modes and at several points of interest indicated in Fig. 3. Particularly, Fig. 4(a) shows the field distribution in the fiber core mode at point A in Fig. 3, which is located far from the point of phase matching with a plasmon (point C in Fig. 3). There, the mode is well-confined to the fiber core with only a little intensity in the PVDF layer region. In Fig. 4(b) we show the field distribution in the plasmonic mode at point B in Fig. 3, which is located far from the phase matching point with the fiber core mode. As expected, most of the modal intensity is concentrated at the PVDF–analyte interface. When the refractive index of analyte increases from $n_a=1.33$ to 1.335, the plasmonic mode shifts toward longer wavelengths [gray dashed curve (red online)].

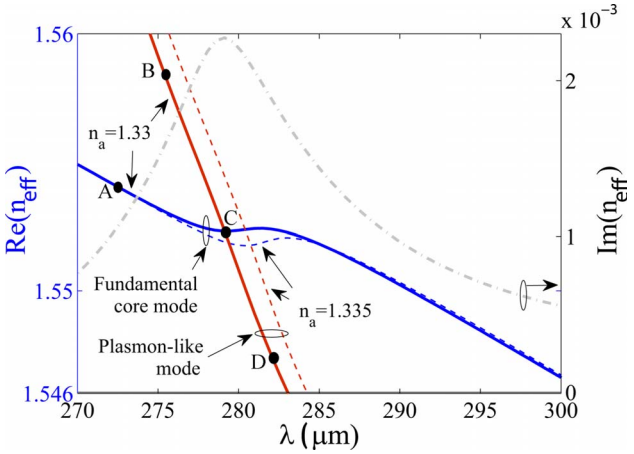


Fig. 3. (Color online) Dispersion relations of the core-guided mode [solid and dashed black curves (blue online)] and the surface plasmon mode [solid and dashed curves running top to bottom (red online)] in the vicinity of the phase-matching point C. Solid curves are calculated for the analyte refractive index $n_a=1.33$, while dashed curves are calculated for $n_a=1.335$. Transmission loss of a core-guided mode (dashed-dotted curve) exhibits a strong increase at the phase-matching point C due to efficient mixing with a plasmon wave.

In Fig. 4(c) we show the field distribution in the core mode at the point C in Fig. 3, which is located exactly at the phase matching point with a plasmon mode. At point C strong mixing between the two modes is observed. Also note that the curvature of the core mode dispersion relation changes in the vicinity of the phase matching point C. Originally, we believed that this change is due to interaction of a core-guided mode with yet another fiber mode. After performing exhaustive simulations with transfer matrix and finite-element codes we are convinced that there is no other mode located in this region. Therefore, we have to conclude that the observed anomaly in the dispersion relation of a core-guided mode is due to the unusually strong and extended interaction of such a mode with a plasmonic mode. Particularly, when plotting the field distribution in the plasmon mode at the point D, which is located far to the right of the phase matching point, we still observe a very strong mixing between the core-guided and plasmonic modes. By studying positions of bandgap edges we find that this behavior of a plasmonic mode is due to the fact that its dispersion relation to the right of a phase matching point C approaches very quickly the edge of a reflector bandgap. In this case, modal penetration of a plasmon mode through the reflector and into the fiber core becomes strongly pronounced. This, in turn, leads to a strong interaction between the plasmon and core-guided modes even far from the phase matching point, and as a consequence, is an anomaly in the core mode dispersion relation.

Finally, the gray dashed–dotted curve in Fig. 3 shows the imaginary part of the effective refractive index of the fundamental core mode, which also defines modal propagation loss due to absorption by the plasmon. In units of decibels/centimeters such a loss is expressed as

$$\alpha[\mathrm{dB/cm}] = \mathrm{Im}(n_{\mathrm{eff}})40\pi/(\lambda[\mathrm{cm}]\log 10)$$
$$= 1819[\mathrm{dB/cm}]\mathrm{Im}(n_{\mathrm{eff}})\nu[\mathrm{THz}]. \quad (2)$$

For example, at 1 THz, $\mathrm{Im}(n_{\mathrm{eff}})\sim 10^{-3}$ defines a $\sim$1.8 dB/cm propagation loss of a fiber mode. Note that in this paper material absorption of the fiber materials have been neglected with an exception of a PVDF layer. In practice, total modal propagation loss will be approximately given by the sum of the bulk loss of a core material and the loss due to coupling to a plasmon excitation.

Figure 5 shows the anomalous dispersion of the fundamental core mode of a Bragg fiber near the phase matching point with a plasmon mode. Due to strong interaction of the fundamental core mode with a plasmon mode, dispersion of a core mode is highly sensitive to the changes in the refractive index of the analyte. For example, assuming analyte refractive index of 1.33, the core mode dispersion achieves its maximum positive value of 60 ps/(nm-km) at 282 $\mu$m [darker curve (blue online)] in Fig. 5). When changing the refractive index of the analyte by $5\times 10^{-3}$ RIU, the core mode dispersion curve shifts towards longer wavelengths resulting in a new value of modal dispersion of −55 ps/(nm km) at 282 $\mu$m [higher-peaked curve (red online)] in Fig. 5). Such a dramatic sensitivity of modal dispersion to changes in the refractive index of analyte can be, in principle, used for sensing through detection of changes in the pulse propagation.

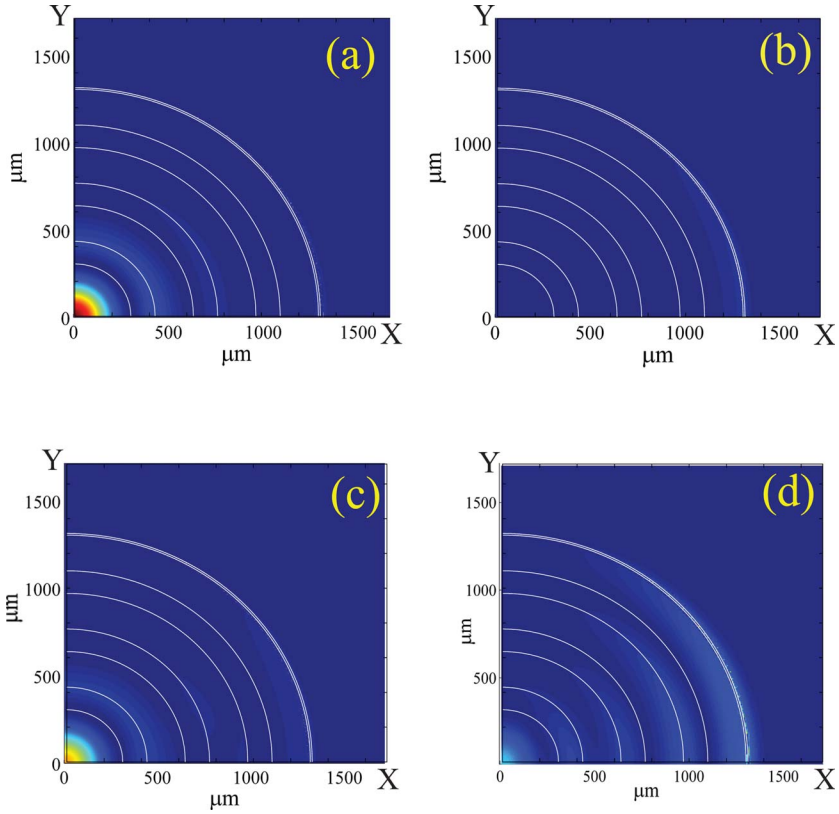


Fig. 4. (Color online) $S_z$ field distributions in the fiber modes at various points indicated in Fig. 3. (a) Fundamental core mode far from the phase matching point. (b) Plasmonic mode far and to the left of the phase matching point. (c) Fundamental core mode at the phase matching point. (d) Plasmonic mode far and to the right of the phase matching point. This mode is located very close to the edge of a reflector bandgap resulting in a strong penetration of a plasmon mode fields into the fiber core.

## 3. SENSITIVITY OF A TERAHERTZ SURFACE-PLASMON-RESONANCE-LIKE SENSOR

Finally, we address the question of sensitivity of a proposed SPR-like sensor to the changes in the refractive index of the analyte. One mode of operation of a proposed sensor is by registering at a fixed frequency the changes in the amplitude of a transmitted light. We define $\alpha(\lambda, n_a)$ to be the transmission loss of the fiber core mode as a function of the wavelength and the refractive index of analyte $n_a$. Considering $P_0$ to be the power launched into the fiber core mode, the power detected after propagation along the sensor of length $L$ will be $P(L,\lambda,n_a) = P_0 \exp(-\alpha(\lambda,n_a)L)$. For the operational wavelength $\lambda$, the amplitude sensitivity to the $dn_a$ change in the analyte refractive index can then be defined as

$$S_A(\lambda)[\mathrm{RIU}^{-1}] = \frac{1}{P(L,\lambda,n_a)} \frac{P(L,\lambda,n_a+dn_a) - P(L,\lambda,n_a)}{dn_a}. \tag{3}$$

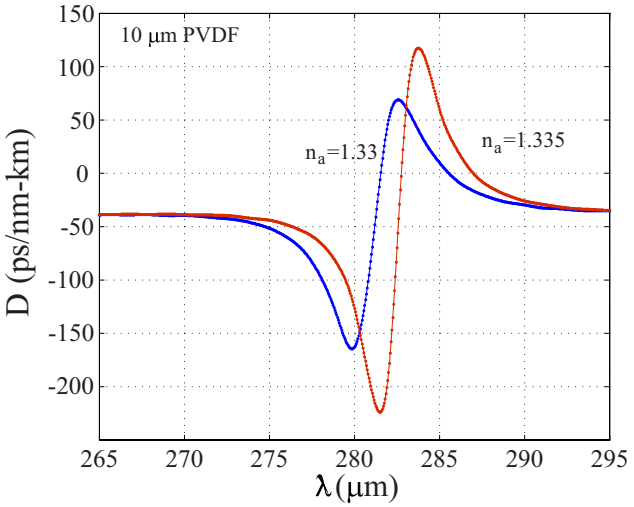


Fig. 5. (Color online) Dispersion of the fundamental core mode near the phase matching point with a plasmon mode for the two values of the analyte refractive index $n_a = 1.33$ and $n_a = 1.335$.

The sensor length $L$ is typically limited by the modal transmission loss. A reasonable choice of a sensor length is $L = 1/\alpha(\lambda, n_a)$; such a choice of sensor length results in a simple definition of sensitivity with respect to small changes in the analyte refractive index,

$$S_A(\lambda)[\mathrm{RIU}^{-1}] = \frac{1}{P(L,\lambda,n_a)} \frac{\partial P(L,\lambda,n_a)}{\partial n_a} = -\frac{1}{\alpha(\lambda,n_a)} \frac{\partial \alpha(\lambda,n_a)}{\partial n_a}. \tag{4}$$

In Fig. 6 we present amplitude sensitivity of a solid-core Bragg fiber sensor presented earlier. The maximal sensitivity is achieved at 285 $\mu$m and is equal to 50 $\mathrm{RIU}^{-1}$. Assuming that one change in the transmitted intensity can be detected reliably, this leads to the sensor resolution of $2 \times 10^{-4}$ RIU. The solid (thin) and dashed black curves in

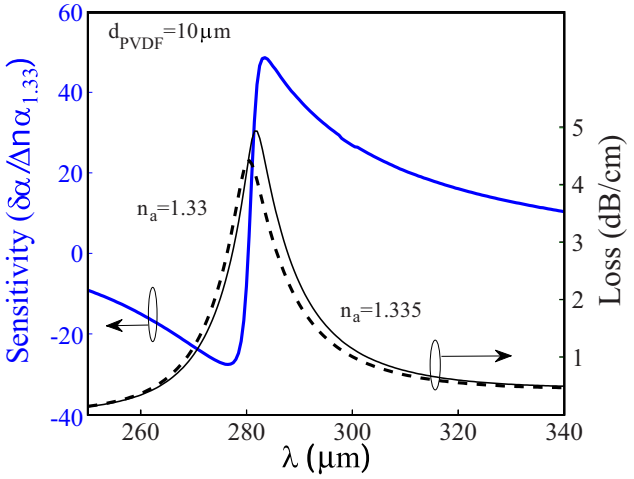


Fig. 6. (Color online) Sensitivity of a solid-core Bragg fiber-based sensor incorporating a thin ferroelectric PVDF layer (thicker solid curve). Loss of a fundamental core mode of a fiber in the vicinity of a phase matching point with a plasmonic mode for the two values of analyte refractive index $n_a = 1.33$ (dashed curve) and $n_a = 1.335$ (solid thin curve).

Fig. 6 show losses of a core guide mode for the two values of the analyte refractive indices. Finally, based on the value of modal losses the sensor length is in the 1 cm range.

## 4. CONCLUSION

In conclusion, the THz plasmonlike excitation on a thin PVDF film via phase matching with a fundamental core mode of a solid-core Bragg fiber is demonstrated. Anomalous dispersion of a core-guided mode due to strong interaction with a plasmonic mode near the band edge of a fiber bandgap is demonstrated. The novel methodology of sensing changes in the refractive index of the analyte via detection of changes in the propagation of short pulses is suggested. Finally, amplitude-based sensor resolution as low as $2 \times 10^{-4}$ RIU is demonstrated in the THz regime, with the sensor length in the 1 cm range.

## REFERENCES

1. V. M. Agranovich and D. L. Mills, *Surface Polaritons—Electromagnetic Waves at Surfaces and Interfaces* (North-Holland, 1982).
2. J. Homola, "Optical fiber sensor based on surface plasmon resonance excitation," Sens. Actuators B **29**, 401–405 (1995).
3. A. Hassani and M. Skorobogatiy, "Design criteria for the microstructured optical fiber-based surface plasmon resonance sensors," J. Opt. Soc. Am. B **24**, 1423–1429 (2007).
4. M. Skorobogatiy and A. V. Kabashin, "Photon crystal waveguide-based surface plasmon resonance biosensor," Appl. Phys. Lett. **89**, 143518 (2006).
5. B. Gauvreau, A. Hassani, M. F. Fehri, A. Kabashin, and M. A. Skorobogatiy, "Photonic bandgap fiber-based surface plasmon resonance sensors," Opt. Express **15**, 11413–11426 (2007).
6. D. Wu, N. Fang, C. Sun, X. Zhang, W. J. Padilla, D. N. Basov, D. R. Smith, and S. Schultz, "Terahertz plasmonic high pass filter," Appl. Phys. Lett. **83**, 201–203 (2003).
7. M. Qiu, "Photonic band structures for surface waves on structured metal surfaces," Opt. Express **13**, 7583–7588 (2005).
8. J. F. O'Hara, R. D. Averitt, and A. J. Taylor, "Prism coupling to terahertz surface plasmon polaritons," Opt. Express **13**, 6117–6126 (2005).
9. K. Wang and D. M. Mittleman, "Dispersion of surface plasmon polaritons on metal wires in the terahertz frequency range," Phys. Rev. Lett. **96**, 157401 (2006).
10. Y. Chen, Z. Song, Y. Li, M. Hu, Q. Xing, Z. Zhang, L. Chai, and C. Y. Wang, "Effective surface plasmon polaritons on the metal wire with arrays of subwavelength grooves," Opt. Express **14**, 13021–13029 (2006).
11. J. G. Rivas, M. Kuttge, H. Kurz, P. H. Bolivar, and J. A. Sanchez-Gil, "Low-frequency active surface plasmon optics on semiconductors," Appl. Phys. Lett. **88**, 082106 (2006).
12. J. W. Lee, M. A. Seo, D. J. Park, D. S. Kim, S. C. Jeoung, Ch. Lienau, Q. H. Park, and P. C. M. Planken, "Shape resonance omni-directional terahertz filters with near-unity transmittance," Opt. Express **14**, 1253–1259 (2006).
13. S. A. Maier, S. R. Andrews, L. Martin-Moreno, and F. J. Garcia-Vidal, "Terahertz surface plasmon-polariton propagation and focusing on periodically corrugated metal wires," Phys. Rev. Lett. **97**, 176805–176807 (2006).
14. F. Miyamaru, M. W. Takeda, T. Suzuki, and C. Otani, "Highly sensitive surface plasmon terahertz imaging with planar plasmonic crystals," Opt. Express **15**, 14804–14809 (2007).
15. J. B. Pendry, A. J. Holden, W. J. Stewart, and I. Youngs, "Extremely low frequency plasmons in metallic mesostructures," Phys. Rev. Lett. **76**, 4773–4776 (1996).
16. J. B. Pendry, A. J. Holden, D. J. Robbins, and W. J. Stewart, "Low frequency plasmons in thin-wire structures," J. Phys.: Condens. Matter **10**, 4785–4809 (1998).
17. T. Hidaka, H. Minamide, H. Ito, J. Nishizawa, K. Tamura, and S. Ichikawa, "Ferroelectric PVDF cladding terahertz waveguide," J. Lightwave Technol. **23**, 2469–2473 (2005).
18. Y. S. Jin, G. J. Kim, and S. G. Jeon, "Terahertz dielectric properties of polymers," J. Korean Phys. Soc. **49**, 513–517 (2006).
19. J. Jin, *The Finite Element Method in Electromagnetics* (Wiley, 2002).